Towards a CFD-PBE simulation of aerated stirred tanks at high gas hold ups and different flow regimes

Towards a CFD-PBE simulation of aerated stirred tanks at high gas hold ups and different flow regimes

Francesco Maluta[a], Alessandro Paglianti[b], Giuseppina Montante[a]

[a]Dipartimento di Chimica Industriale 'Toso Montanari', Alma Mater Studiorum – Università di Bologna, via Terracini 34, 40131, Bologna, Italy

[b]Dipartimento di Ingegneria Civile, Chimica, Ambientale e dei Materiali, Alma Mater Studiorum – Università di Bologna, via Terracini 34, 40131, Bologna, Italy

Abstract

In this work we analyze the challenges of the adoption of a population balance approach in aerated stirred tanks operating at high gas volume fractions, in different flow regimes and when segregation of the phases is present, i.e. due to the formation of aerated cavities behind flat blades. A decoupled solution of the equations governing the fluid flow and of the population balance equation (PBE) is adopted to obtain preliminary information on the bubble size distribution and to identify the specific issues that need to be addressed to extend the applicability of the population balance model to different regimes. A workflow is proposed for the simulation of aerated stirred tanks with geometries for which established correlations for the estimation of bubble size are not available and a simplified approach to determine whether a coupled CFD PBE solution may be required is presented.

1 Introduction

The numerical simulation of gas-liquid stirred tank is a powerful tool for the design and analysis in a wide range of applications (Shi and Rzehak, 2018), including fermentation, polymerization, oxidation, biotechnological processes, to name a few (Middleton and Smith, 2004). One of the Computational Fluid Dynamics (CFD) main advantages is that local information on the two phase flow field and the related properties can be obtained, thus allowing for the detailed description and troubleshooting of the processes (Montante et al., 2008), provided that a robust and reliable modelling approach is adopted.

One of the most challenging aspects of the CFD simulation of gas-liquid stirred tank concerns the accurate prediction of the bubble size distribution (BSD) in the system. The BSD determines the gas-liquid flow field, hence the power consumption and the gas-liquid flow regime that in turn affect the BSD, thus coupling the phenomena inside the system, increasing the modelling complexity of such unit operations (Petitti et al., 2013). One way to simplify the simulation of gas-liquid stirred tank consists in adopting a single bubble diameter representative of the fluid dynamics in the system to obtain information on the main features of the flow (Lane et al., 2002). Such approach has recently proved successful in predicting the aerated cavities forming behind the flat blades of the impeller, such as in Rushton turbines, (Cappello et al., 2021; Maluta et al., 2021a), and the shape and size of such cavities reached a good agreement with experimental data and established correlations (Maluta et al., 2021b). The accurate prediction of the aerated cavities is important since the power drawn by the impeller depends on the formation of such structures (Warmoeskerken et al., 1981) and the reliable prediction of the power consumption is paramount in industrial applications and for scale-up/scale-down purposes.

Despite these recent improvement in the simulations of gas-liquid stirred tank, the main drawback of a single bubble diameter approach is in the determination of the specific interfacial area for the interphase mass transfer. To obtain the interfacial area in the context of the Two Fluid Model (TFM) either simplified arithmetical models (Maluta et al., 2019) or a population balance approach can be adopted. Several studies addressed the description of the BSD solving a population balance equation (PBE), but this approach is often limited to complete dispersed systems in the complete recirculation regime, as qualitatively shown in Figure 1, where the operative conditions of selected studies from the literature analyzing aerated tanks stirred with Rushton turbines are plotted as a function of the gas flow number, $Fl_G = Q_G/ND^3$, and the impeller Froude number, $Fr = N^2D/g$, with Q_G being the gas flow rate, N and D being the impeller rotational speed and diameter respectively and g being the gravitational acceleration.

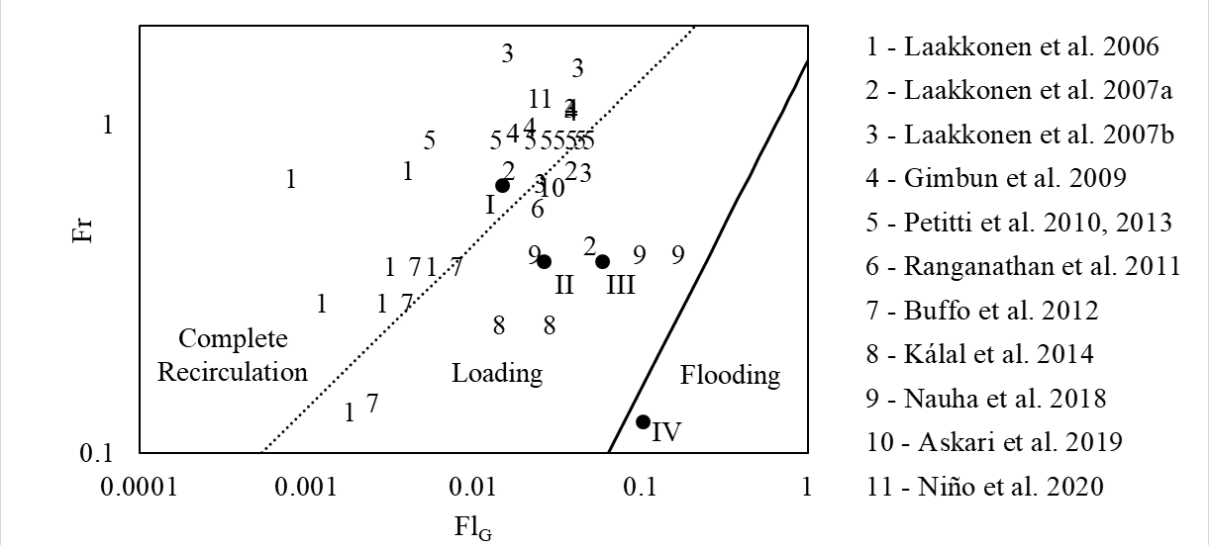

Figure 1 – Flow regimes map and operative conditions considered in this work (circles with roman numerals) and in selected literature studies on the simulations of gas-liquid stirred tanks with a population balance approach (numbers).

In Figure 1 the lines represent the regime transitions as obtained from the correlations developed by Nienow et al. (1985, 1977) and the flow map holds when the baffled stirred tanks have a standard geometry and the same ratio of $D/T = 1/3$, with T being the tank diameter, and in case of multiple Rushton impellers, the flow regime is referring to the lowest impeller. In particular, Laakkonen et al. (2006) experimentally characterized a tank stirred by a Rushton turbine in which bubbles were injected by means of a porous sparger and validated the PBE with a compartment model approach in which local information on the flow field was derived from single phase CFD simulations. A similar approach was used in a successive work (Laakkonen et al., 2007a) in which a ring sparger was used and gas-liquid simulations were performed to pass information to the compartment model and eventually this approach allowed the analysis of the interphase mass transfer (Laakkonen et al., 2007b). Gimbun et al. (2009) validated the BSD obtained from the solution of the PBE with a Quadrature method of moments (QMOM) with the results of Laakkonen et al. (2007a) and analyzed the interphase mass transfer coefficient, $k_L a$, in different tank scales. Petitti et al. (2010) developed a robust formulation of the QMOM approach, validating their prediction with the results by Laakkonen et al. (2007a, 2006), successively extending their prediction to the interphase mass transfer of the system sparged with the porous sparger with a multidimensional population balance model (Buffo et al., 2012; Petitti et al., 2013). A dual impeller gas-liquid stirred tank was studied by Ranganathan and Sivaraman (2011), validating the BSD with results from the literature, and the same system in the same operative conditions was also simulated by Kerdouss et al. (2006) and Selma et al. (2010). The main shortcoming in these works is that no information is given on the bubble size exiting the sparger, its geometry or type. Kálal et al. (2014) studied the effect of spatial discretization and drag laws on the

computational model predictions, collecting experimental BSD for validation, while Nauha et al. (2018) studied a 100m^3 multi-impeller fermenter in, which the lowest Rushton turbine was in the loading regime, with the compartment approach developed by Laakkonen et al. (2007a). Askari et al. (2019) compared the local profiles of water velocity obtained from their CFD-PBE simulations with results from Deen et al. (2002). The works by Kálal et al. (2014), Nauha et al. (2018) and Askari et al. (2019) analyzed the stirred tank in the loading conditions, but no information were given concerning the prediction of the aerated cavities. In the same work, Askari et al. (2019) also analyzed a tank stirred by a three bladed marine propeller, the latter in complete recirculation, loading and flooding conditions, but the spatial distributions of gas volume fraction in this configuration did not fully agree with their experimentally detected flow regimes. More recently Niño et al. (2020) studied a tank stirred by a Rushton turbine and modified the breakage and the coalescence kernels to account for the complete turbulence spectrum, validating their results with purposely collected experimental data.

Despite the increasing literature concerning the description of stirred tank with a population balance approach and the different aspects investigated, the study of such systems is mostly limited to the complete recirculation regime or loading conditions close to the regime transition to complete recirculation. In the loading regime, the formation of the aerated cavities and the relative decrease in power drawn by the impeller is not mentioned. This would limit the applicability of such modelling approach to industrial systems that are often operated in different regimes and for which the power consumption is a fundamental parameter (Noorman et al., 2018). Moreover, in different flow regimes the local two-phase fluid dynamics varies considerably inside the stirred tank and the breakup and coalescence mechanisms may change depending on the local conditions (Liao and Lucas, 2010, 2009). The coalescence and breakup kernels must therefore manage to describe those phenomena in such diverse conditions. A further limitation arises from the computational times, that for coupled CFD PBE simulations may become prohibitively long, especially when large scale geometries are adopted.

In this work, the goal is to identify and analyze the modelling challenges and the limitations to overcome in order to obtain reliable results from CFD simulations coupled with PBE of gas-liquid stirred tanks in different flow regimes. The study set foot from a validated computational approach (Maluta et al., 2021b, 2021c) that proved successful in predicting the gas-liquid fluid dynamics with a single bubble diameter and original data of the system in different flow regimes are presented (solid points in Figure 1). Decoupling the solution of the PBE from the gas-liquid flow field allows to understand the limitations and the sources of error that need to be addressed before obtaining realistic predictions from a fully predictive CFD-PBE coupled solution also in the case of very inhomogeneous two-phase flow conditions in the vessel volume, as is the case of impeller blades with aerated cavities and loading/flooding regimes. Firstly the investigated

gas-liquid stirred tank is described and successively the computational model to obtain the gas-liquid flow field is presented, together with the equations to obtain the bubble size with empirical correlations from the literature and with a population balance approach. The PBE predictions are then presented and discussed, focusing on the differences in the bulk of the system and in the impeller zone in conditions with and without formation of aerated cavities. The volumetric distribution of the bubble Sauter mean diameter is analyzed and a workflow for the simulation of aerated stirred tanks is proposed. Finally, conclusions based on the results are drawn.

2 The gas-liquid stirred tank

The system analyzed in this work is a cylindrical flat-bottomed tank of diameter T=0.23m equipped with four equally spaced baffles and stirred by means of a Rushton turbine of diameter D=T/3 positioned at an off-bottom clearance of C=T/2. The tank is filled with water up to a height equal to the tank diameter, H_L=T. The injection of air ($\rho_G = 1.225$ kg/m^3) in water ($\rho_L = 998$ kg/m^3, $\mu_L = 0.001$ Pa·s) is achieved through a ring sparger of diameter 0.4D and positioned at an off-bottom distance of T/5. The ring sparger distributes the gas through 10 equally spaced circular holes of diameter equal to 1mm, positioned on its upper side.

Four operative conditions were investigated, corresponding to three different gas-liquid flow regimes in the tank, identified through the correlations developed by Nienow et al. (1985, 1977). A stirring speed of 550rpm and a gas flow rate of 221L/h (Fl_G=0.015, Fr=0.657), produce a compete recirculation regime (I in Figure 1) without the formation of aerated cavities, reducing the impeller speed to 421rpm (Fr=0.385), and simultaneously increasing the gas flow rate to 300L/h, (Fl_G=0.026), and 664L/h, (Fl_G=0.058), changes the regime to loading, in which vortex-clinging cavities, VC (II in Figure 1), are observed at the lowest gas flow rate and small '3-3' cavities at the highest (III in Figure 1) . The last flow regime investigated is the flooding regime and it was obtained with a gas flow rate of 664L/h and an impeller rotational speed of 240rpm, (Fl_G=0.102, Fr=0.125) (IV in Figure 1). The operative conditions described above are reported as circles in Figure 1.

3 CFD Model

The presented computational model was proposed and validated in previous studies (Maluta et al., 2021b, 2021c) and it proved successful in predicting the main features of the two-phase flow, such as the shape and size of the aerated cavities, the power consumption and the flow regimes. The fluid dynamics of the system presented in Section 2 was modelled with the steady state, isothermal, incompressible Reynolds Averaged Navier Stokes (RANS) equations, extended to two phases with the so-called Two-Fluid model (TFM), and for the generic *i-th* phase they read as:

$$\nabla \cdot (\alpha_i \rho_i \boldsymbol{u_i}) = 0 \quad (1)$$

$$\nabla \cdot (\alpha_i \rho_i \boldsymbol{u_i} \boldsymbol{u_i}) = -\alpha_i \nabla P + \alpha_i \rho_i \boldsymbol{g} + \nabla \cdot (\boldsymbol{\tau_i} + \boldsymbol{\tau_i^t}) + \boldsymbol{F_D} + \boldsymbol{F_{TD}} \quad (2)$$

With α_i being the volume fraction and $\boldsymbol{u_i}$ being the velocity of the relative fluid. P is the pressure shared by the phases, $\boldsymbol{\tau_i}$ and $\boldsymbol{\tau_i^t}$ are the viscous and Reynolds stress tensor, respectively. The multiphase $k-\varepsilon$ turbulence model was adopted to close the set of equations, obtaining the mixture turbulent viscosity, μ_t, from phase averaged properties (mixture formulation), as already done in similar studies (Buffo et al., 2012; Petitti et al., 2010) resulting in:

$$\mu_t = 0.09 \rho_{mix} k^2 / \varepsilon \quad (3)$$

With ρ_{mix} being the phase-averaged mixture density, k being the turbulent kinetic energy and ε being the turbulent kinetic energy dissipation rate. The last two terms in Eq. 2 are the interphase momentum transfer terms, namely the interphase drag force and the turbulent dispersion force, respectively.

As successfully done in previous works (Maluta et al., 2021b, 2021c), the interphase forces were expressed in terms of the bubble terminal velocity only, U_t, as originally proposed by Scargiali et al. (2007), and both the continuous and disperse volume fractions were included in the force formulation, to limit the forces at high gas hold ups (Maluta et al., 2021a). The drag force, $\boldsymbol{F_D}$, thus becomes:

$$\boldsymbol{F_D} = \frac{\alpha_L \alpha_G}{U_t^2} \boldsymbol{g} (\rho_L - \rho_G) \| \boldsymbol{u_G} - \boldsymbol{u_L} \| (\boldsymbol{u_G} - \boldsymbol{u_L}) \quad (4)$$

With the subscripts L and G indicating properties referred to the liquid and gas phase, respectively.

The turbulent dispersion force, $\boldsymbol{F_{TD}}$, was modelled with the Burns model (Burns et al., 2004) and it reads:

$$\boldsymbol{F_{TD}} = \frac{\alpha_L \alpha_G}{U_t^2} \boldsymbol{g} (\rho_L - \rho_G) \| \boldsymbol{u_G} - \boldsymbol{u_L} \| \left[\frac{\mu_t}{\rho_L \sigma_{t,L}} \left(\frac{\nabla \alpha_G}{\alpha_G} - \frac{\nabla \alpha_L}{\alpha_L} \right) \right] \quad (5)$$

Where $\sigma_{t,L}$ indicates the eddy viscosity Prandtl number, which assumed a value of 0.9.

In determining the two-phase flow field, a single bubble terminal velocity was assumed, meaning that a monodistributed bubble diameter, d_{32}, is considered in each of the conditions studied in this work. The bubble terminal velocity was calculated with the Grace model, described in Clift et al. (2005), and its expression is:

$$U_t = \frac{\mu_L}{\rho_L d_{32}} Mo^{-0.149} \left(C_1 \left[\frac{4}{3} Eo \, Mo^{-0.149} \right]^{\beta} - 0.857 \right) \quad (6)$$

The Morton number is defined as $Mo = \mu_L^4 g(\rho_L - \rho_G)/(\rho_L^2 \sigma^3)$, with σ being the surface tension of water, equal to 0.072N/m, and the Eötvös number is $Eo = g(\rho_L - \rho_G)d_{32}^2/\sigma$. When the term in square brackets assumes values between 2 and 59.3, the parameters C_1 and β become 0.94 and 0.757 respectively, while C_1 and β are equal to 3.42 and 0.441 when the term in square brackets is larger than 59.3. The Grace model describes the terminal velocity of ellipsoidal bubbles when $Mo < 10^{-3}$, $Eo < 40$ and $Re_B > 0.1$, with the bubble Reynolds numbers defined as $Re_B = U_t \rho_L d_{32}/\mu_L$. Additionally, Eq. 6 can describe the spherical bubbles terminal velocity if $Re_B < 300$ (Clift et al., 2005).

3.1 Bubble size calculation

As explained in Section 3, a single terminal velocity and hence a single bubble diameter was assumed to obtain the gas-liquid flow field. As done in previous works (Maluta et al., 2021b, 2021c), just the bubble diameter in the impeller zone, that is the impeller swept volume, was adopted to obtain the gas-liquid flow field, and it was calculated with the correlations developed by Alves (Alves et al., 2002) with the following equation:

$$d_{32} = 0.25 \left(\frac{Pg}{V_I}\right)^{-0.52} \quad 7$$

With Pg being the gassed power drawn by the impeller, and V_I being the volume swept by the impeller equal to $V_I = \pi/20\, D^3$. The correlation holds for superficial gas velocities, $U_{sup} = Q_G/(T^2\, \pi/4)$, lower than 2×10^{-3} m/s, and this condition is satisfied by each of the conditions studied in this work. For superficial gas velocities higher than said threshold, the correlation developed by Alves to obtain the bubble diameter in the impeller zone in coalescing systems at high gas flow rates can be adopted:

$$d_{32} = 8.5(1 + 32.5 \frac{Q_G}{D^2}) \left(\frac{Pg}{V_I}\right)^{-0.24} \quad 8$$

Together with the correlations to obtain the diameter in the impeller zone, Alves et al. (2002) developed correlations to obtain the d_{32} in the bulk of aerated tanks stirred with a Rushton turbine. This correlation for coalescing systems has the following expression:

$$d_{32} = 0.0076 \left(\frac{Pg}{V}\right)^{-0.14} \quad 9$$

where V is the volume of the tank. In this work Eq.8 and Eq.9 where not used to obtain the bubble diameter adopted in Eq. 6 and they are reported here for sake of completeness and to compare the results of the simulations with known correlations.

In baffled gas-liquid stirred tanks similar to the one adopted in this work, correlations to obtain the gassed power consumption were developed by Smith et al. (1987), combining information on the gassed cavities, flow regimes and empiricism (Nienow, 1998; Smith et al., 1987).

In aerated stirred tanks with the formation of vortex-clinging cavities behind the blades of the Rushton impeller, the relative power demand, $RPD = Pg/Pu$, that is the ratio of the gassed to ungassed, Pu, power consumption, can be obtained with the following expression:

$$\frac{Pg}{Pu} = 1 - 16.7 Fl_G Fr^{0.35} \qquad 10$$

On the other hand, when small '3-3' cavities develop, the following expression can be adopted:

$$\frac{Pg}{Pu} = B + (A - B)\frac{Fl_G - 0.1}{(Fl_G)_{3-3} - 0.1}$$
$$A = 1 - 17(Fl_G)_{3-3} Fr^{0.35} \qquad 11$$
$$B = 0.27 + 0.022/Fr$$

Where $(Fl_G)_{3-3} = 0.0038(Re^2/Fr)^{0.07} T^{0.5}/D^{0.5}$ is a threshold gas flow number at which the transition between vortex-clinging and small '3-3' cavities is expected (Warmoeskerken et al., 1981), and it is function of the impeller Reynolds number, $Re = ND^2\rho_L/\mu_L$.

3.2 Population balance equation

Once the steady state gas-liquid flow field was obtained with a single bubble diameter with the methodology described in Section 3 and 3.1, a population balance equation, PBE, was solved in each of the operative conditions described in Section 2 to obtain preliminary information on the BSD needed to calculate the specific interfacial area. The PBE solved in this work reads:

$$\frac{\partial n}{\partial t} + \nabla \cdot (\mathbf{u_G} n) = B_B^B + B_B^C - D_B^B - D_B^C \qquad 12$$

Where n is the bubble number density function (NDF) and the terms B_B and D_B are the sum of birth and death rate of bubbles due to breakage (B) and coalescence (C) phenomena. The solution of the PBE was decoupled from the solution of the equations governing the fluid flow, therefore, the gas volume fraction and the gas velocities in Eq. 12 are not modified by the evolution of the bubble size.

The bubble birth rate due to breakup reads:

$$B_B^B(d) = \int_{d_B}^{\infty} \beta(d, d')\, g(d') n(d) \mathrm{d}d' \qquad 13$$

While the bubble death rate due to breakup is:

$$D_B^B(d) = g(d)n(d) \quad (14)$$

With β being the daughter distribution function describing the size distribution of droplets, d, originating from the breakup of a bubble with diameter equal to d' and g being the breakup frequency. The breakage phenomena are described with the model developed by Laakkonen et al. (2006), and binary breakup was assumed. The daughter size distribution thus reads:

$$\beta(d, d') = 180\left(\frac{d^2}{d'^3}\right)\left(\frac{d^3}{d'^3}\right)^2\left(1 - \frac{d^3}{d'^3}\right)^2 \quad (15)$$

The breakup frequency is defined as:

$$g(d') = C_1\varepsilon^{1/3} erfc\left(\sqrt{C_2\frac{\sigma}{\rho_L\varepsilon^{2/3}d'^{5/3}} + C_3\frac{\mu_L}{\sqrt{\rho_L\rho_G}\varepsilon^{1/3}d'^{4/3}}}\right) \quad (16)$$

With $C_2 = 0.04$ and $C_3 = 0.01$ being model parameters which values were assumed equal to those proposed by Laakkonen et al. (2006), and $C_1 = 6.0$, as proposed by Petitti et al. (2010) for a similar system.

The bubble birth rate due to coalescence is defined as:

$$B_B^C(d) = \frac{1}{2}\int_0^{d_B} a\left((d^3 - d'^3)^{1/3}, d'\right) n(d) n\left((d^3 - d'^3)^{1/3}\right) \mathrm{d}d' \quad (17)$$

While the death rate due to coalescence reads:

$$D_B^C(d) = \int_0^{\infty} a(d, d') n(d) n(d') \mathrm{d}d' \quad (18)$$

Where a is the coalescence kernel modelling the coalescence frequency. To describe the coalescence mechanism, the model developed by Coulaloglou and Tavlarides (1977) with an algebraic correction was adopted (Prince and Blanch, 1990):

$$a(d, d') = 0.88\varepsilon^{1/3}(d + d')^2\left(d^{2/3} + d'^{2/3}\right)^{1/2}\eta(d, d') \quad (19)$$

With $\eta(d, d')$ being the coalescence efficiency of two colliding bubbles defined as:

$$\eta(d, d') = \exp\left(-C_4\frac{\mu_L\rho_L\varepsilon}{\sigma^2}\left(\frac{d\,d'}{d + d'}\right)^4\right) \quad (20)$$

Where the parameter $C_4 = 6.0 \times 10^9$ contains information regarding the initial and final critical thickness of the liquid film between the two colliding bubbles (Petitti et al., 2010).

As extensively done in the literature (Gimbun et al., 2009; Maluta et al., 2021d; Petitti et al., 2013, 2010; Shiea et al., 2020), the PBE was solved with the Quadrature Method of Moments, simplifying the NDF with a quadrature approximation. The quadrature nodes and weights were obtained from the first 6 moments of the NDF (Buffo et al., 2012) with the well-known Product-Difference algorithm (Marchisio and Fox, 2013).

3.3 Numerical solution

The equations presented in Section 3 were solved by ANSYS Fluent 2020 in a computational domain matching the geometry described in Section 2. The domain was discretized in 2 million hexahedral cells, thus ensuring the grid independency of the turbulent variables, based on previous results obtained in single phase systems (Coroneo et al., 2011; Maluta et al., 2021d). The relative motion between steady and rotating walls was modelled with the multiple reference frame approach. No-slip boundary conditions were imposed for both phases on the solid walls, the only exception being the upper surface of the air sparger for which a velocity inlet was assumed just for the gas phase. The top surface of the tank was modelled with a degassing boundary condition, which acts as a mass sink for the gas phase and a free-slip boundary condition for the liquid phase. A pseudo-transient solver was adopted to numerically solve the set of equations in the domain in each of the operative conditions described in Section 2. The second order upwind scheme was adopted to discretize the momentum and the transport of turbulent variables equations, while the QUICK scheme was used for the volume fraction transport equation. For the pressure-velocity coupling the pressure-based coupled algorithm was adopted. This configuration and numerical set up was used to characterize and validate the formation of cavities and their size in different regimes in a previous work (Maluta et al., 2021b).

The solution of the PBE presented in Section 3.3 was decoupled from the CFD equations solution described earlier in this Section. No-flux boundary conditions were assumed for all the NDF moments on the surfaces in the domain, except for the upper part of the air sparger. Here the moments of a delta distribution centered on the size of the bubbles exiting the sparger obtained with the correlation by Geary and Rice (1991) were adopted as boundary conditions for the NDF moments. The bubble diameters exiting the sparger obtained from the correlation by Geary and Rice (1991) ranged from 7.1mm to 7.8mm, depending on the operative conditions considered. An implicit transient solver with time steps of 10^{-3}s was adopted to solve the NDF moment transport equations, discretized with a second order upwind scheme.

4 Results and Discussion

In this section the results concerning the solution of the PBE in the steady state mean flow field obtained with the TFM using a single bubble diameter are presented. The starting point is the gas-liquid fluid dynamics obtained with the bubble diameter in the impeller zone estimated by Eq. (7). The fluid dynamics results obtained with this approach were already validated in previous works (Maluta et al., 2021c, 2021b) and are not reported here for brevity.

Firstly, the prediction of the PBE without phase segregation, i.e., the aerated cavities, are presented and successively the analysis is extended to operative conditions in which the two phases locally segregate. The analysis continues presenting the volumetric distribution of the Sauter mean diameter in the four conditions considered and lastly a workflow for the simulation of gas-liquid stirred tanks when established correlations for bubble size are not available is presented.

The constant bubble size obtained with Eq.7 and the relative bubble terminal velocity, Eq.6, adopted to obtain the two-phase flow field are reported in Table 1. The fluid dynamics results were validated and discussed in previous works, hence they are not shown here for brevity, and the reader can refer to (Maluta et al., 2021b) for further information.

Table 1 – Bubble sizes and terminal velocities adopted for the CFD simulations, as obtained from the Alves correlations in the impeller zone

Flow regime	Case	N - rpm	Q_G – L/h	d_{32} - mm	U_t – cm/s
Complete recirculation	I	550	221	0.6	6.2
Loading (VC cavities)	II	421	300	1.0	11.8
Loading (‘3-3’ cavities)	III	421	664	1.4	15.6
Flooding	IV	240	664	2.1	20.5

When comparing the bubble diameters predicted by the simulations with the values obtained from correlations (Eq.7 and Eq.9), the diameter in the bulk was obtained as a mass average of the bubble diameters in the whole volume, while the bubble diameter in impeller zone was calculated at an axial coordinate equal to T/2 and at a radial distance from the center of the tank equal to 0.25T, to match the sampling zone in the work by Alves et al. (2002). The computed gas hold up in the system is equal to 2.04% for the case in complete recirculation conditions, 1.66% and 2.41% for the system in the loading regime with the formation of VC and ‘3-3’ cavities, respectively, and 1.45% in the flooding regime.

4.1 Predictions of bubble size in the system without phase segregation

The solution of the PBE described in Section 3.2 for the case of complete recirculation regime and without cavities, Case I, led to the prediction of a mass average Sauter mean diameter, d_{32}, in the impeller and in the bulk zone of tank equal to 2.4 mm and 2.6 mm, respectively. The corresponding values obtained with Eq. 7 and Eq.9 are 0.6mm and 3.0mm, respectively. The deviation of 20% in the bulk of the tank is consistent with the predictions by other authors (Laakkonen et al., 2007a; Petitti et al., 2013) and this difference leads to a deviation of 12% in the bubble terminal velocity as obtained with Eq.6. Therefore, in this case the differences in the predictions of the bubble diameter in the bulk have a larger effect on the resulting k_La, with respect to the gas-liquid fluid dynamics. Instead, the significant difference obtained in the impeller zone questions the ability of the population balance model to accurately predict the bubble size distribution in gas-liquid systems at high gas flow rates in the proximity of the impeller. Since the bubble size in the impeller zone is crucial for a correct prediction of the gas-liquid flow regimes and the gassed power consumption and in the literature very few numerical and experimental studies analyze this aspect, the phenomena involved in the definition of the bubble size distribution may need further investigation. In the relatively small volume swept by the impeller, the turbulent dissipation rate is usually much higher than in the rest of the tank, the gas hold up can reach very high values, being the air sparger positioned just below the stirrer, and the experimental determination of the bubble size distribution is difficult due to the rotation of the impeller. These difficulties reflect on the PBE and especially on the kernels needed to model coalescence and breakup. Analyzing two of the most widely adopted coalescence kernels, namely the model proposed by Coulaloglou and Tavlarides (1977) and the one proposed by Prince and Blanch (1990) for bubble columns but adopted also in the simulation of gas-liquid stirred tanks (Gimbun et al., 2009; Niño et al., 2020) very different behaviors are observed at high turbulent dissipation rates, typically close to the impeller, and results of the predictions of these two models from the literature are shown in Figure 2 for a range of turbulent dissipation rates usually found in turbulent stirred tanks and a range of bubble sizes expected in the system, to highlight the different behavior in such equipment.

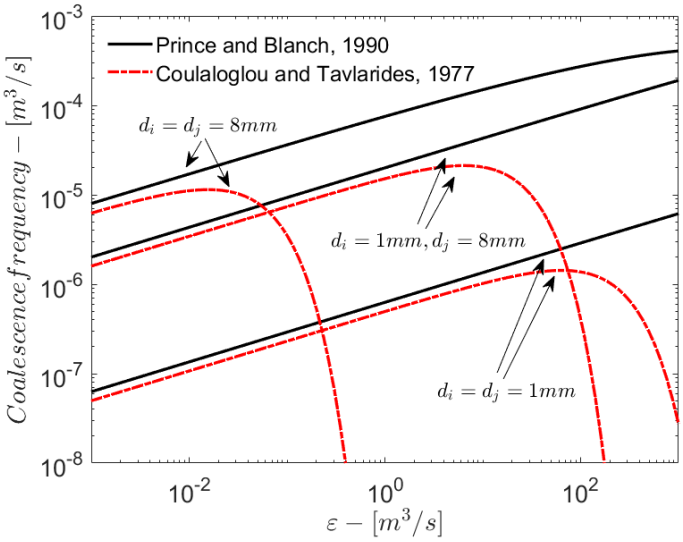

Figure 2 – Comparison between coalescence frequencies as predicted by different kernels as a function of the turbulent dissipation rate and the diameters of two colliding bubbles with diameter equal to d_i and d_j

Figure 2 shows that at high turbulence dissipation rates the behavior of the two coalescence kernels is very different, while at lower ε the two kernels predict a similar coalescence frequency. In the operative conditions considered, the mass weighted turbulence dissipation rate in the impeller zone is equal to 27m^3/s^2, with local maxima higher than 200 m^3/s^2, therefore the choice of the most suitable kernel is paramount in predicting the evolution of the bubbles in the impeller zone, considering that both smaller bubbles recirculated from the bulk (represented by the bubbles with diameter equal to 1mm) and larger bubbles coming from the air sparger are present (represented by the bubbles with diameter equal to 8mm). Figure 2 introduces another aspect that strongly affects the BSD in the impeller zone, namely the diameter of the bubbles reaching it. To investigate the effect of this parameter, a local comparison between the d_{32} in the impeller zone and in the bulk obtained from two simulations with different sizes of the bubbles exiting the sparger were performed and the results are shown in Figure 3. The correlation by Geary and Rice (1991) predicted bubbles with diameter equal to 7.1mm (Large Bubbles, LB), while a balance of bubble buoyancy against interfacial tension without considering inertia or viscosity effects, as adopted by Askari et al. (2019) and Kerdouss et al. (2008), predicted bubble diameter of 3.5mm (Small Bubbles, SB).

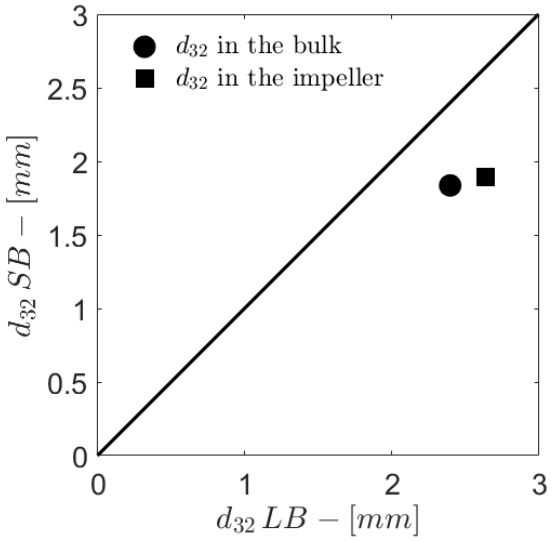

Figure 3 – Comparison between the Sauter mean diameter in the bulk and in the impeller zone for N=550rpm and QG=221L/h, Case I, as obtained with a bubble size exiting the sparger calculated with the correlation by Geary and Rice (1991) (LB) and with a simplified force balance (SB)

Figure 3 shows that the size of the bubble exiting the sparger has a smaller influence on the d_{32} in the bulk of the tank with respect to the predictions of the d_{32} in the impeller zone, moreover the predicted bubble size in the impeller region is higher than in the bulk, despite the higher turbulent dissipation rate. Having adopted the coalescence kernel by Coulaloglou and Tavlarides (1977) that limits the coalescence rate at high turbulent dissipation rates, large d_{32} in the impeller zone may results from an insufficient breakup of bubbles coming from the sparger. This suggests that the breakup kernel struggles in predicting the breakage phenomena of large bubbles. Some of the most cited experiments in the literature adopt a porous sparger (Laakkonen et al., 2006) that generates smaller bubbles, compared to ring spargers, while experiments performed with a ring sparger (Laakkonen et al., 2007a) do not report the bubble size close to the impeller, therefore accurate experimental data are needed to address this aspect.

The accurate prediction of the bubble size in the impeller zone is not a crucial problem when just the determination of the specific interfacial area for interphase mass transfer in complete recirculation condition is of interest. On the other hand, an overestimation of the bubble size in the impeller when aerated cavities are expected may lead to wrong cavities shape and size (Maluta et al., 2021b) consequently failing in predicting the gassed power consumption and possibly the gas-liquid flow field.

4.2 Predictions of bubble size in the system with phase segregation

The comparison between the Sauter mean diameter in the bulk as obtained from the correlation, Eq.9, and as predicted by the PBE as a mass average in the whole domain is shown in Figure 4 for all the operative conditions considered in this work, including the conditions without aerated cavities described in Section 4.1.

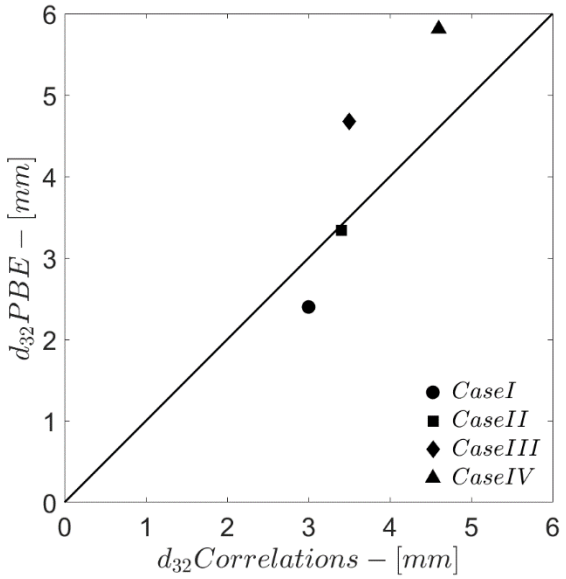

Figure 4 – Mass averaged Sauter mean diameter in the whole system as obtained from the PBE and from the correlation, Eq.9, in different operative conditions

Figure 4 shows that a fair agreement is obtained for results averaged in the whole domain for both cases where segregation of the two phases is present and where it is not. The maximum deviation from the correlation is 32% and it is observed in the case stirred at N=421rpm and with a gas flow rate of 664L/h, Case III, that corresponds to loading conditions where small '3-3' cavities develop, nevertheless also in this worst case the maximum deviation between the terminal velocity for the bubbles from the correlation and from the PBE is less than 3%, being the terminal velocity of bubbles in the ellipsoidal regime almost constant. From this result it follows that the bubble size distribution as predicted with the PBE would lead to fluid dynamics predictions close to those obtained with a single bubble diameter, being the differences between the terminal velocity of the bubbles based on the d_{32} predicted with the PBE and estimated with the correlation almost negligible, even at high gas flow rates and when segregation occurs.

A completely different conclusion is obtained from the analysis of the results in the impeller zone as shown in Figure 5.

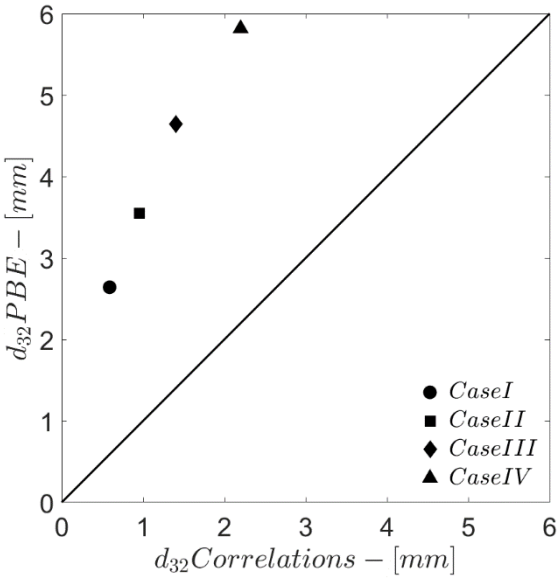

Figure 5 – Mass averaged Sauter mean diameter in the impeller zone as obtained from the PBE and from the correlation, Eq.7, in different operative conditions

Figure 5 shows that the bubble size predicted by the PBE substantially differs from the results obtained with Eq. 7, as also observed in the system without phase segregation. When aerated cavities form behind the blades of the impeller the agreement worsens. On top of the limitations already discussed in Section 4.1, the additional issue of the turbulence description in the impeller zone must be addressed.

As already pointed out, Eq.3 gives the turbulent viscosity as a function of the averaged properties of the gas-liquid flow. Adopting this formulation of the turbulence modelling, high turbulent dissipation rates are predicted inside the aerated cavities. The mass average of turbulent dissipation rate in the system is very weakly affected by these high local values, being the density of the gas phases 3 orders of magnitude lower than the liquid density, therefore the power number as obtained from the mass integral of ε gives results in agreement with experimental data and established correlations (Maluta et al., 2021b). Local high values of turbulence dissipation rate in the gas phase, however, may alter the BSD predictions with the PBE, resulting in further uncertainties to the adoption of this approach in segregated gas-liquid systems. A previous study (Maluta et al., 2021a) addressed the difference in the predictions by different multiphase formulations of the $k - \varepsilon$ model, but no substantial differences were observed in the predicted power numbers. Adopting different formulations of the multiphase turbulence model still produces high turbulent dissipation rates in the aerated cavities, therefore more fundamental study is required to address the issue and expanding the validity of the RANS multiphase turbulence models. The formulation of reliable multiphase turbulence models together with the development of specific kernels to describe the breakup and coalescence mechanisms in such gas-liquid flows, and especially when there is segregation of the phases, is a

fundamental prerequisite to the adoption of a reliable CFD-PBM coupled approach. In fact, the correct prediction of the bubble terminal velocity in the impeller zone, which is function of the bubble size, is an imperative precondition to obtain accurate gas-liquid fluid dynamics in aerated fermenters (Maluta et al., 2021c).

4.3 Volume distribution of Sauter mean diameter

The solution of the PBE in a flow field obtained with a single bubble diameter can provide important information on the overall volume distribution of the bubble size, and in particular on the Sauter mean diameter distribution. The analysis of the d_{32} allows to gather preliminary knowledge on the expected average specific interfacial area, being its physical interpretation the ratio of the bubble volume to surface area, as well as the average interphase forces, being their formulations dependent on this property. The d_{32} distribution and the ε distribution on a vertical plane midway two consecutive baffles are shown in Figure 6 together with the aerated cavities forming behind the blades of the impeller, identified as those cells in which the gas volume fraction is higher than 0.95. In complete recirculation conditions, Case I, Figure 6a, small differences exist between the bubbles above the impeller plane and those below it. In particular, smaller bubbles are found in the lower part of the tank. The distribution of turbulent dissipation rate in this case is similar to the single phase, with maximum values in the discharge jet from the turbine where the trailing vortexes from the impeller blades develop, high values where the jet impinges against the lateral walls of the tank and small but not negligible values in the bulk of the system. A similar ε distribution is found in the loading conditions as well, Figure 6b, Case II, and Figure 6c, Case III, with overall lower values. In fact, the presence of the cavities limits the pumping capacity of the impeller and the large amount of gas deflects the discharge jet towards the upper part of the tank. Almost negligible turbulent dissipation values are found in the bulk of the system. The lower turbulent dissipation rate and the higher gas flow rates reflect on the gas volume fraction and Sauter mean diameter distribution. Just small bubbles are entrained in the lower loops below the impeller plane and overall large diameters are found in the upper part of the tank, where increasing radial gradients of bubble size become observable. In the flooding condition, Figure 6d, Case IV, the pumping capacity of the impeller are drastically reduced, and the bubbles barely break, resulting in large bubble diameters in the whole system. The discharge jet is evidently deflected by the gas motion, the turbulent intensity inside the jet is noticeably lower than in the other regimes and the high turbulent dissipation rate close to the vessel wall almost disappears, leaving the majority of the vessel volume with very low turbulent dissipation values.

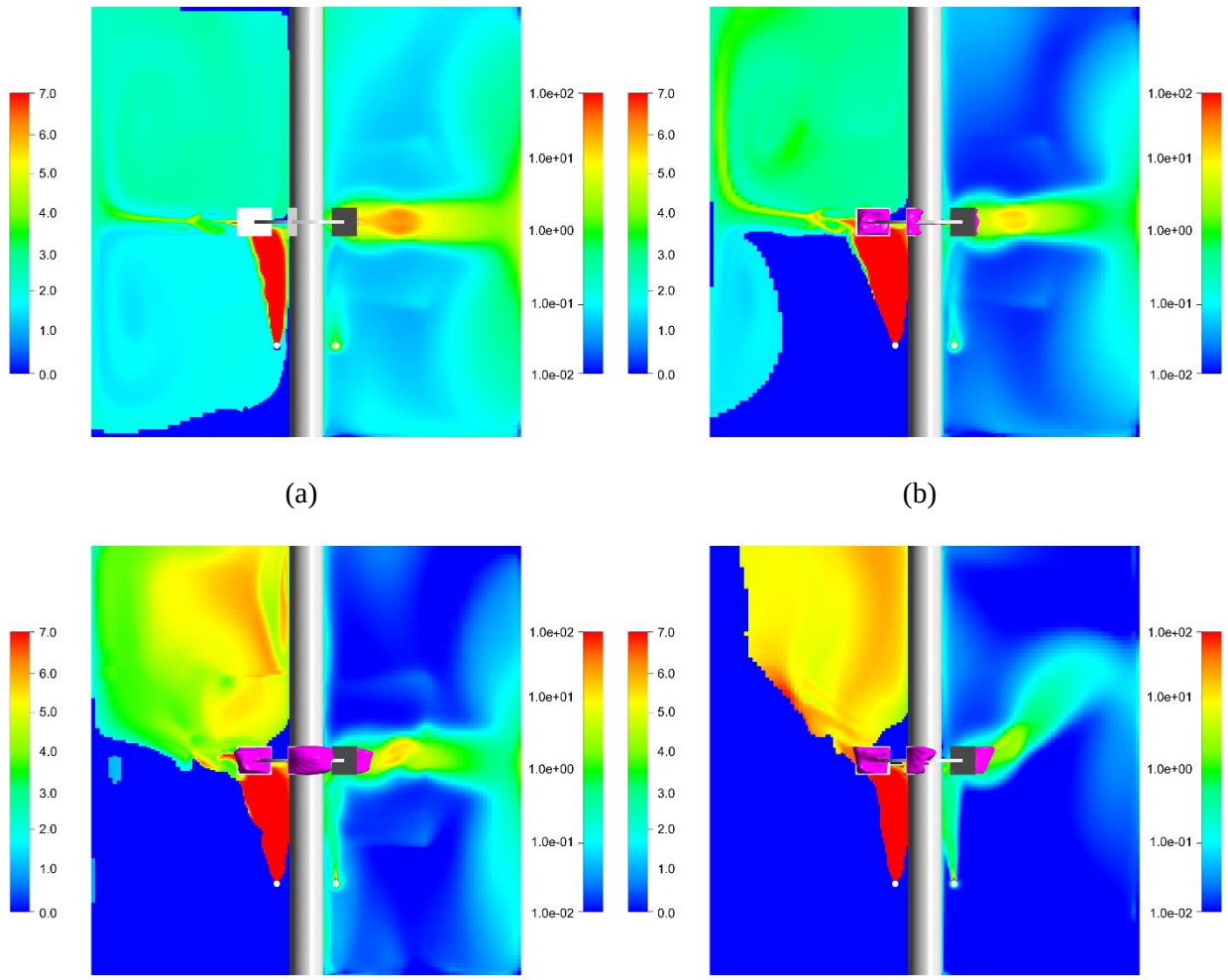

Figure 6 – Sauter mean diameter in mm (left) and turbulent dissipation rate in m^2/s^3 (right) distributions on a vertical plane midway two consecutive baffles in Case I (a), Case II (b), Case III (c) and Case IV (d). Cells with gas volume fractions higher than 0.95 (aerated cavities) are displayed in purple.

The volumetric distribution of d_{32} obtained from the simulations performed in this work is reported in Figure 7 as a volume weighted probability.

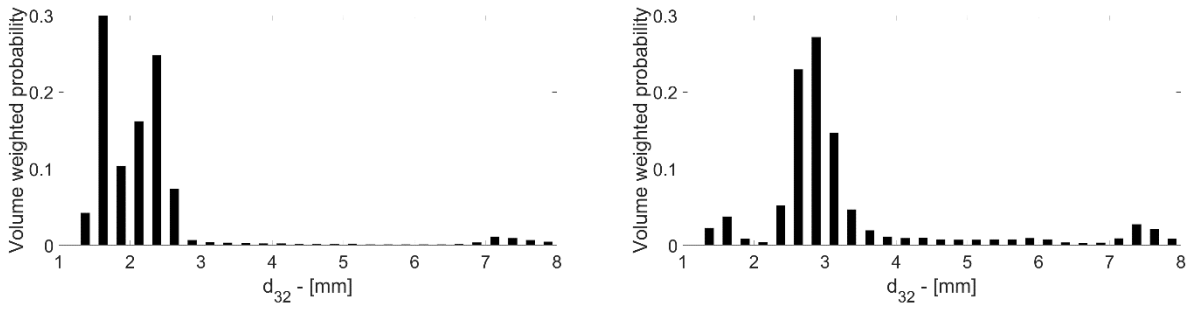

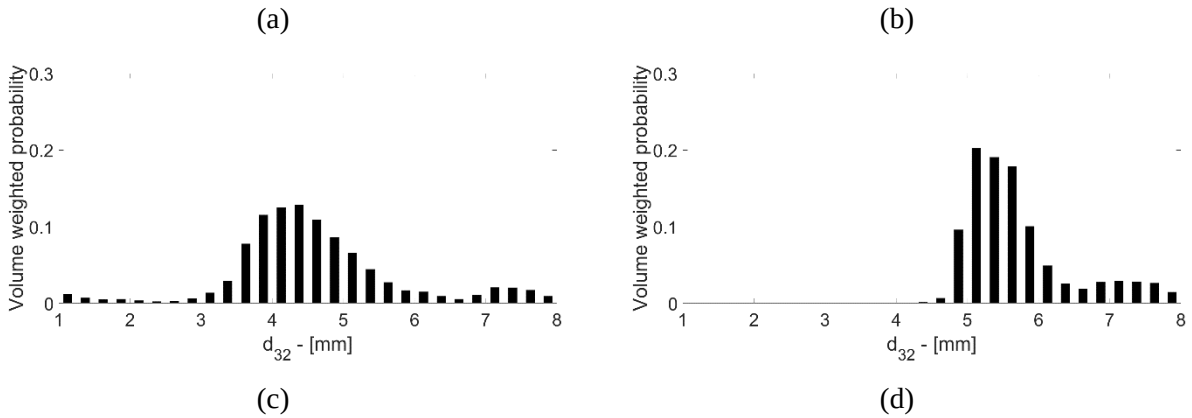

Figure 7 – Volumetric d_{32} distributions obtained in Case I (a), Case II (b), Case III (c) and Case IV (d) in the whole volume.

Figure 7a shows that in complete recirculation conditions, Case I, more than 80% of the bubble volume consist of bubbles with Sauter mean diameter between 1.6mm and 2.4mm, and the corresponding terminal velocities range from 17cm/s and 22cm/s. Despite the relatively narrow distribution, the predicted bubble shapes span both in the spherical and in the ellipsoidal regime, therefore a simplified description of the system with a single diameter obtained from this analysis may lead to important differences both in the specific interfacial area and in the two-phase flow field. Figure 7b, on the other hand, shows that in loading regime where clinging cavities develop, Case II, more than 70% of the bubble volume consists of bubbles with d_{32} ranging from 2.4mm and 3.1mm, and the corresponding terminal velocities lay between 22cm/s and 25cm/s. These bubbles are ellipsoidal, and since their terminal velocity is very similar, the system may be described with a single bubble diameter, without resolving to a two-way coupling between CFD and PBE, provided that the main features of the flow were correctly predicted. To obtain a realistic description of the interphase specific area of the two operative conditions at higher gas flow rate, namely in the loading regime with the formation of '3-3' cavities, Case III, Figure 7c and in the flooding regime, Case IV, Figure 7d, a single bubble diameter seems insufficient, since the Sauter mean diameter distribution spans several millimeters. Interestingly enough, being the bubbles in the ellipsoidal regime, their terminal velocities vary very little, with values between 23cm/s and 25cm/s, meaning that the description of the gas-liquid flow field with a single bubble diameter is sufficient. These results suggest that the analysis on the predicted bubble size must include both the bubble diameter distribution, especially for the determination of the specific interfacial area, and the calculations of the bubble terminal velocities, since wide bubble size distributions spanning several millimetres may produce narrow bubble terminal velocity distributions.

4.4 Workflow for gas-liquid simulations in different stirred tank geometries

The computational approach presented in Section 3 relies on the determination of the gas-liquid flow field with a single bubble diameter obtained from the correlations developed by Alves et al. (2002) in gas-liquid

stirred tanks of standard geometries, stirred with a single Rushton turbine, and this approach proved robust and reliable (Maluta et al., 2021b, 2021c). In this Section a procedure to obtain the bubble diameter when the correlations developed by Alves et al. (2002) are outside their range of validity is proposed and validated and a workflow to determine whether or not a single bubble diameter may be sufficient is presented.

The starting point of this procedure is the determination of the bubble diameter in the impeller zone, since it was demonstrated that this size allows to satisfactorily predict the main features of the flow, such as flow regimes, cavities size and shape and the consecutive impeller power consumption (Maluta et al., 2021b). The PBE presented in Section 3.2 was solved in the vessel geometry considering a single value of turbulent dissipation rate and with an initial bubble size, significantly higher than the bubble sizes expected in the system, equal to 10mm. The CFD solver is thus used as a differential equation solver with lumped parameters, since the two-phase turbulent velocity field was initialized with a value equal to 0 and the respective differential equations were not solved. To validate this first step of the procedure, the single value of the turbulent dissipation rate, $< \varepsilon >$, was obtained assuming that the power predicted either by Eq.10 or Eq.11 was dissipated in the volume swept by the impeller. The results for each of the conditions considered in this work are shown in Table 2.

Table 2 – Average turbulent dissipation rate, Sauter mean diameter from the lumped parameter solution of the PBE and the relative Alves correlations predictions in the impeller zone adopted for the CFD simulations.

Case	N - rpm	Q_G – L/h	$< \varepsilon >$ - m^2/s^3	d_{32} from PBE - mm	d_{32} from Alves - mm
I	550	221	113.2	0.7	0.6
II	421	300	44.3	1.1	1.0
III	421	664	32.6	1.2	1.4
IV	240	664	5.2	1.9	2.2

Table 2 shows that the predictions of the lumped solution of the PBE and the results from the correlations are in very good agreement, therefore such approach can be used to obtain the bubble diameter in the impeller zone, required to perform the gas-liquid simulations with the procedure in Section 3. When the correlations to obtain the power consumption cannot be adopted, a single phase simulation may be run, obtaining the average turbulent dissipation rate in the volume swept by the impeller. Since this value would be likely overestimating the actual $< \varepsilon >$, the resulting bubble diameter will be smaller than the expected. Nonetheless, this value may be used to determine a first guess of the gas-liquid flow field, thus obtaining a new value of $< \varepsilon >$ that can be used to perform a new calculation with the lumped solution of the PBE. This procedure may necessitate few iterations to obtain a constant bubble value.

Once obtained the gas-liquid flow field with the constant bubble diameter, the decoupled solution of the PBE as presented in Section 4.1 and Section 4.2 would provide a preliminary insight on the bubble size

distribution. Moreover, analyzing the volumetric Sauter mean diameter distribution and especially calculating the expected bubble terminal velocities, it would be possible to discriminate whether a CFD PBE coupled solution may be needed or not. In fact, if a monodistributed bubble terminal velocity distribution is obtained, the flow field description with a single bubble diameter may be sufficient and the decoupled solution of the PBE would give information on the expected specific interfacial area. Conversely, if a large range of bubble terminal velocities is obtained, a coupled solution of CFD equations and PBE may improve the predictions of the gas-liquid flow field as well as the specific interfacial area, provided that the issues highlighted in Section 4.1 and Section 4.2 are accounted for. The proposed workflow is schematically shown in Figure 8.

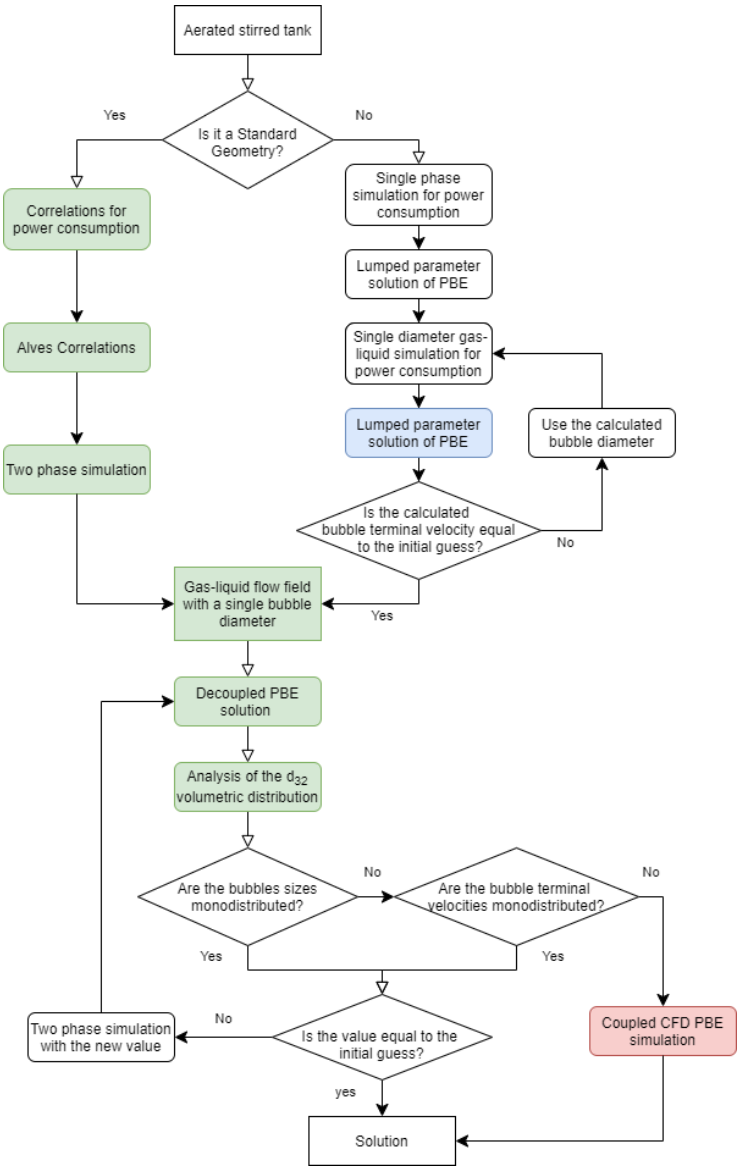

Figure 8 – Workflow for the simulation of aerated stirred tanks. Green tiles are highlight the procedure adopted in this work, the blue tile was validated in Section 4.4 and the red tile highlights open issues that must be addressed to obtain reliable results. Tiles with rounded edges are instructions, tiles with sharp edges are results

Figure 8 provides a workflow to guide towards the simulation of aerated stirred tanks. The procedure adopted in this manuscript is highlighted by the green tiles: dealing with a standard geometry, correlations for calculating the power consumption (Eq.10, Eq. 11) were adopted, the bubble diameter in the impeller zone was obtained with the Alves correlations (Eq.7, Eq. 8) and two-phase simulations were performed to obtain the gas liquid flow field with a single bubble diameter, and the fluid dynamics results were validated in previous works. The analysis of the Sauter mean diameter from the decoupled CFD-PBM simulation highlighted that further modelling efforts must be carried out before reliably predicting the two-phase flow

field in such conditions and a coupled CFD-PBM simulation would return incorrect results (red tile in Figure 8). The procedure is especially interesting when industrial geometries (i.e. non-standard geometries) are adopted. In fact, the lumped parameter solution of the PBE (blue tile in Figure 8) returned results in good agreement with the correlations by Alves, Table 2, also highlighting that the Population balance allows to obtain results in agreement with the experimental correlations when the advection contribution is neglected, provided that a realistic value of turbulent dissipation rate is adopted.

5 Conclusions

In this work, a workflow for the simulation of aerated stirred tanks is developed, starting from the critical analysis of the applicability of a population balance approach in determining the BSD in several operating conditions. Most of the studies on the topic published in the literature analyze the complete recirculation flow regime in which no gas accumulation is expected, as in the case of cavities behind the blades of the Rushton impeller. In this study the limitations in extending this approach to different conditions including highly segregated gas zones are studied.

In particular, a PBE solved with QMOM was solved in a stationary gas-liquid turbulent flow field obtained with a single bubble diameter derived from established correlations for four different operative conditions, thus decoupling the solution of the PBE and the equation governing the flow. The approach revealed that the Sauter mean diameter predicted in the bulk of the system for different conditions substantially agrees with the correlations by Alves et al. (2002), therefore this approach can be used to obtain preliminary information on the specific interfacial area. On the other hand, in the impeller zone the numerical predictions disagree with the results of the correlations, hence breakup and coalescence kernels need further development to address this aspect. The multiphase turbulence modelling in the impeller zone must be improved as well, especially when aerated cavities develop. High quality experimental data in the impeller zone is needed to improve the predictions and provide a benchmark for the validation of the models. The correct prediction of the BSD in the impeller zone is particularly important when a fully coupled CFD PBE approach is needed, since a wrong prediction of the bubble diameters in this zone may lead to erroneous flow fields.

The decoupled solution proposed in this work underlines the importance of considering the bubble terminal velocities distribution, as well as the BSD, and a procedure is proposed to determine whether a fully coupled solution is needed. The procedure also shows a way to obtain a flow field with a single bubble diameter when established correlations are not applicable.

Future works will investigate the numerical and experimental analysis of aerated fermenters in equipment and in operating conditions closer to those typically adopted in industrial operations.

6 References

Alves, S.S., Maia, C.I., Vasconcelos, J.M.T., Serralheiro, A.J., 2002. Bubble size in aerated stirred tanks. Chem. Eng. J. 89, 109–117. https://doi.org/10.1016/S1385-8947(02)00008-6

Askari, E., St-Pierre Lemieux, G., Proulx, P., 2019. Application of extended quadrature method of moments for simulation of bubbly flow and mass transfer in gas-liquid stirred tanks. Can. J. Chem. Eng. 97, 2548–2564. https://doi.org/10.1002/cjce.23470

Buffo, A., Vanni, M., Marchisio, D.L., 2012. Multidimensional population balance model for the simulation of turbulent gas–liquid systems in stirred tank reactors. Chem. Eng. Sci. 70, 31–44. https://doi.org/10.1016/j.ces.2011.04.042

Burns, A.D., Frank, T., Hamill, I., Shi, J.-M.M., 2004. The Favre Averaged Drag Model for Turbulent Dispersion in Eulerian Multi-Phase Flows, in: Fifth International Conference on Multiphase Flow, ICMF-2004. Yokohama, Japan, pp. 1–17.

Cappello, V., Plais, C., Vial, C., Augier, F., 2021. Scale-up of aerated bioreactors: CFD validation and application to the enzyme production by Trichoderma reesei. Chem. Eng. Sci. 229, 116033. https://doi.org/10.1016/j.ces.2020.116033

Clift, R., Grace, J.R., Weber, M.E., 2005. Bubbles, drops, and particles, 1st ed. Dover Publications, Inc., Mineola, New York.

Coroneo, M., Montante, G., Paglianti, A., Magelli, F., 2011. CFD prediction of fluid flow and mixing in stirred tanks: Numerical issues about the RANS simulations. Comput. Chem. Eng. 35, 1959–1968. https://doi.org/10.1016/j.compchemeng.2010.12.007

Coulaloglou, C.A., Tavlarides, L.L., 1977. Description of interaction processes in agitated liquid-liquid dispersions. Chem. Eng. Sci. 32, 1289–1297. https://doi.org/10.1016/0009-2509(77)85023-9

Deen, N.G., Solberg, T., Hjertager, B.H., 2002. Flow Generated by an Aerated Rushton Impeller: Two-phase PIV Experiments and Numerical Simulations. Can. J. Chem. Eng. 80, 1–15. https://doi.org/10.1002/cjce.5450800406

Geary, N.W., Rice, R.G., 1991. Bubble size prediction for rigid and flexible spargers. AIChE J. 37, 161–168. https://doi.org/10.1002/aic.690370202

Gimbun, J., Rielly, C.D., Nagy, Z.K., 2009. Modelling of mass transfer in gas–liquid stirred tanks agitated by Rushton turbine and CD-6 impeller: A scale-up study. Chem. Eng. Res. Des. 87, 437–451. https://doi.org/10.1016/j.cherd.2008.12.017

Kálal, Z., Jahoda, M., Fořt, I., 2014. Modelling of the Bubble Size Distribution in an Aerated Stirred Tank: Theoretical and Numerical Comparison of Different Breakup Models. Chem. Process Eng. 35, 331–348. https://doi.org/10.2478/cpe-2014-0025

Kerdouss, F., Bannari, A., Proulx, P., 2006. CFD modeling of gas dispersion and bubble size in a double turbine stirred tank. Chem. Eng. Sci. 61, 3313–3322. https://doi.org/10.1016/j.ces.2005.11.061

Kerdouss, F., Bannari, A., Proulx, P., Bannari, R., Skrga, M., Labrecque, Y., 2008. Two-phase mass transfer coefficient prediction in stirred vessel with a CFD model. Comput. Chem. Eng. 32, 1943–1955. https://doi.org/10.1016/j.compchemeng.2007.10.010

Laakkonen, M., Alopaeus, V., Aittamaa, J., 2006. Validation of bubble breakage, coalescence and mass transfer models for gas–liquid dispersion in agitated vessel. Chem. Eng. Sci. 61, 218–228. https://doi.org/10.1016/j.ces.2004.11.066

Laakkonen, M., Moilanen, P., Alopaeus, V., Aittamaa, J., 2007a. Modelling local bubble size distributions in agitated vessels. Chem. Eng. Sci. 62, 721–740. https://doi.org/10.1016/J.CES.2006.10.006

Laakkonen, M., Moilanen, P., Alopaeus, V., Aittamaa, J., 2007b. Modelling Local Gas–Liquid Mass Transfer in Agitated Vessels. Chem. Eng. Res. Des. 85, 665–675. https://doi.org/10.1205/cherd06171

Lane, G.L., Schwarz, M.P., Evans, G.M., 2002. Predicting gas–liquid flow in a mechanically stirred tank. Appl. Math. Model. 26, 223–235. https://doi.org/10.1016/S0307-904X(01)00057-9

Liao, Y., Lucas, D., 2010. A literature review on mechanisms and models for the coalescence process of fluid particles. Chem. Eng. Sci. 65, 2851–2864. https://doi.org/10.1016/j.ces.2010.02.020

Liao, Y., Lucas, D., 2009. A literature review of theoretical models for drop and bubble breakup in turbulent dispersions. Chem. Eng. Sci. 64, 3389–3406. https://doi.org/10.1016/j.ces.2009.04.026

Maluta, F., Buffo, A., Marchisio, D., Montante, G., Paglianti, A., Vanni, M., 2021a. Effect of turbulent kinetic energy dissipation rate on the prediction of droplet size distribution in stirred tanks. Int. J. Multiph. Flow 136, 103547. https://doi.org/10.1016/j.ijmultiphaseflow.2020.103547

Maluta, F., Paglianti, A., Montante, G., 2021b. Two-fluids RANS predictions of gas cavities, power consumption, mixing time and oxygen transfer rate in an aerated fermenter scale-down stirred with multiple impellers. Biochem. Eng. J. 166, 107867. https://doi.org/10.1016/j.bej.2020.107867

Maluta, F., Paglianti, A., Montante, G., 2021c. Prediction of gas cavities size and structure and their effect on the power consumption in a gas-liquid stirred tank by means of a two-fluid RANS model. Chem. Eng. Sci. 241, 116677. https://doi.org/10.1016/j.ces.2021.116677

Maluta, F., Paglianti, A., Montante, G., 2021d. Prediction of Gas-filled Cavity Structures in Aerated Vessels stirred with multiple Rushton Turbines. Chem. Eng. Trans. 86, 1135–1140. https://doi.org/10.3303/CET2186190

Maluta, F., Paglianti, A., Montante, G., 2019. Modelling of biohydrogen production in stirred fermenters by Computational Fluid Dynamics. Process Saf. Environ. Prot. 125, 342–357. https://doi.org/10.1016/j.psep.2018.09.020

Marchisio, D.L., Fox, R.O., 2013. Computational Models for Polydisperse Particulate and Multiphase Systems, Cambridge University Press. Cambridge University Press, Cambridge. https://doi.org/10.1017/CBO9781139016599

Middleton, J.C., Smith, J.M., 2004. Gas-liquid mixing in turbulent systems, in: Paul, E.L., Atiemo-Obeng, V.A., Kresta, S.M. (Eds.), Handbook of Industrial Mixing: Science and Practice. John Wiley & Sons Inc., Hoboken, New Jersey, pp. 585–638.

Montante, G., Horn, D., Paglianti, A., 2008. Gas–liquid flow and bubble size distribution in stirred tanks. Chem. Eng. Sci. 63, 2107–2118. https://doi.org/10.1016/j.ces.2008.01.005

Nauha, E.K., Kálal, Z., Ali, J.M., Alopaeus, V., 2018. Compartmental modeling of large stirred tank bioreactors with high gas volume fractions. Chem. Eng. J. 334, 2319–2334. https://doi.org/10.1016/j.cej.2017.11.182

Nienow, A.W., 1998. Hydrodynamics of Stirred Bioreactors. Appl. Mech. Rev. 51, 3–32. https://doi.org/10.1115/1.3098990

Nienow, A.W., Warmoeskerken, M.M.C.G., Smith, J.M., Konno, M., 1985. On the flooding/loading transition and the complete dispersal condition in aerated vessels agitated by a Rushton-turbine, in: Proc. of the 5th European Conf. on Mixing. BHRA Fluid Engineering, Wurzburg, Germany, pp. 143–154.

Nienow, A.W., Wisdom, D.J., Middleton, J.C., 1977. The effect of scale and geometry on flooding, recirculation, and power in gassed stirred vessels, in: Proc. of the 2nd European Conf. on Mixing. BHRA Fluid Engineering, Mons, BE, pp. F1-1-F1-16.

Niño, L., Gelves, R., Ali, H., Solsvik, J., Jakobsen, H., 2020. Applicability of a modified breakage and coalescence model based on the complete turbulence spectrum concept for CFD simulation of gas-liquid mass transfer in a stirred tank reactor. Chem. Eng. Sci. 211, 115272. https://doi.org/10.1016/j.ces.2019.115272

Noorman, H.J., van Winden, W., Heijnen, J.J., van der Lans, R.G.J.M., 2018. CHAPTER 1. Intensified

Fermentation Processes and Equipment, in: RSC Green Chemistry. Royal Society of Chemistry, pp. 1–41. https://doi.org/10.1039/9781788010320-00001

Petitti, M., Nasuti, A., Marchisio, D.L., Vanni, M., Baldi, G., Mancini, N., Podenzani, F., 2010. Bubble size distribution modeling in stirred gas-liquid reactors with QMOM augmented by a new correction algorithm. AIChE J. 56, 36–53. https://doi.org/10.1002/aic.12003

Petitti, M., Vanni, M., Marchisio, D.L., Buffo, A., Podenzani, F., 2013. Simulation of coalescence, break-up and mass transfer in a gas–liquid stirred tank with CQMOM. Chem. Eng. J. 228, 1182–1194. https://doi.org/10.1016/j.cej.2013.05.047

Prince, M.J., Blanch, H.W., 1990. Bubble coalescence and break-up in air-sparged bubble columns. AIChE J. 36, 1485–1499. https://doi.org/10.1002/aic.690361004

Ranganathan, P., Sivaraman, S., 2011. Investigations on hydrodynamics and mass transfer in gas–liquid stirred reactor using computational fluid dynamics. Chem. Eng. Sci. 66, 3108–3124. https://doi.org/10.1016/j.ces.2011.03.007

Scargiali, F., D'Orazio, A., Grisafi, F., Brucato, A., 2007. Modelling and Simulation of Gas–Liquid Hydrodynamics in Mechanically Stirred Tanks. Chem. Eng. Res. Des. 85, 637–646. https://doi.org/10.1205/cherd06243

Selma, B., Bannari, R., Proulx, P., 2010. Simulation of bubbly flows: Comparison between direct quadrature method of moments (DQMOM) and method of classes (CM). Chem. Eng. Sci. 65, 1925–1941. https://doi.org/10.1016/j.ces.2009.11.018

Shi, P., Rzehak, R., 2018. Bubbly flow in stirred tanks: Euler-Euler/RANS modeling. Chem. Eng. Sci. 190, 419–435. https://doi.org/10.1016/j.ces.2018.06.001

Shiea, M., Buffo, A., Vanni, M., Marchisio, D., 2020. Numerical Methods for the Solution of Population Balance Equations Coupled with Computational Fluid Dynamics. Annu. Rev. Chem. Biomol. Eng. 11, 339–366. https://doi.org/10.1146/annurev-chembioeng-092319-075814

Smith, J.M., Warmoeskerken, M.M.C.G., Zeef, E., 1987. Flow conditions in vessels dispersing gases in liquids with multiple impellers, in: Ho, C.S., Oldshue, J.Y. (Eds.), Biotechnology Processes: Scale-up and Mixing. American Institute of Chemical Engineers, New York, pp. 107–115.

Warmoeskerken, M.M.C.G., Feijen, J., Smith, J.M., 1981. Hydrodynamics and power consumption in stirred gas-liquid dispersions., in: FLUID MIXING SYMPOSIUM. Institution of Chemical Engineers, BRADFORD, U.K., pp. J1-B14.